AGU PUBLICATIONS

Global Biogeochemical Cycles

RESEARCH ARTICLE
10.1002/2016GB005408

Key Points:
- Continental dust input to the ocean is reconstructed using thorium isotopes
- A new global data base of dust fluxes is presented for the late Holocene and the Last Glacial Maximum
- Comparisons with recent coupled models identify regions of good model-data agreement

Supporting Information:
- Supporting Information S1
- Data Set S1

Correspondence to:
S. S. Kienast,
stephanie.kienast@dal.ca

Citation:
Kienast, S. S., G. Winckler, J. Lippold, S. Albani, and N. M. Mahowald (2016), Tracing dust input to the global ocean using thorium isotopes in marine sediments: ThoroMap, *Global Biogeochem. Cycles*, *30*, doi:10.1002/2016GB005408.

Received 4 MAR 2016
Accepted 25 SEP 2016
Accepted article online 28 SEP 2016

Tracing dust input to the global ocean using thorium isotopes in marine sediments: ThoroMap

S. S. Kienast[1], G. Winckler[2,3], J. Lippold[4,5], S. Albani[6,7], and N. M. Mahowald[6]

[1]Department of Oceanography, Dalhousie University, Halifax, Nova Scotia, Canada, [2]Lamont-Doherty Earth Observatory, Columbia University, Palisades, New York, USA, [3]Department of Earth and Environmental Sciences, Columbia University, Palisades, New York, USA, [4]Institute of Geological Sciences and Oeschger Centre for Climate Change Research, University of Bern, Bern, Switzerland, [5]Institute of Earth Sciences, University of Heidelberg, Heidelberg, Germany, [6]Department of Earth and Atmospheric Sciences, Cornell University, Ithaca, New York, USA, [7]Institute for Geophysics and Meteorology, University of Cologne, Cologne, Germany

Abstract Continental dust input into the ocean-atmosphere system has significant ramifications for biogeochemical cycles and global climate, yet direct observations of dust deposition in the ocean remain scarce. The long-lived isotope thorium-232 (^{232}Th) is greatly enriched in upper continental crust compared to oceanic crust and mid-ocean ridge basalt-like volcanogenic material. In open ocean sediments, away from fluvial and ice-rafted sources of continental material, ^{232}Th is often assumed to be of predominantly eolian origin. In conjunction with flux normalization based on the particle reactive radioisotope thorium-230 (^{230}Th), ^{232}Th measurements in marine sediments are a promising proxy for dust accumulation in the modern and past ocean. Here we present ThoroMap, a new global data compilation of ^{230}Th-normalized fluxes of ^{232}Th. After careful screening, we derive dust deposition estimates in the global ocean averaged for the late Holocene (0–4 ka) and the Last Glacial Maximum (LGM, 19–23 ka). ThoroMap is compared with dust deposition estimates derived from the Community Climate System Model (CCSM3) and CCSM4, two coupled atmosphere, land, ocean, and sea ice models. Model-data correlation factors are 0.63 (CCSM3) and 0.59 (CCSM4) in the late Holocene and 0.82 (CCSM3) and 0.83 (CCSM4) in the LGM. ThoroMap is the first compilation that is built on a single, specific proxy for dust and that exclusively uses flux-normalization to derive dust deposition rates.

1. Introduction

Continental dust, or mineral aerosol, plays a significant role in the climate system. Dust particles affect the Earth's radioactive balance by both scattering and absorbing incoming solar radiation and outgoing planetary radiation [e.g., *Boucher et al*., 2013]. Additionally, dust particles act as cloud condensation nuclei, and feldspars, in particular, as ice nuclei [*Atkinson et al*., 2013]; clouds in turn affect planetary albedo. Dust deposition to snow and ice surfaces can significantly increase their melting rates by decreasing their albedo [*Conway et al*., 1996]. Last but not least, iron-bearing dust profoundly influences the biological uptake of CO_2 not only in the terrestrial biosphere but also in large parts of the ocean where dissolved iron has unequivocally been shown to limit phytoplankton production [e.g., *Boyd et al*., 2007].

Many lines of evidence suggest that mineral dust has been an important player in the unperturbed climate system in the past and that it will be one in the future [e.g., *Werner et al*., 2002; *Mahowald et al*., 2006; *Martinez-Garcia et al*., 2009, 2011; *Winckler et al*., 2005, 2008, 2016; *Maher et al*., 2010; *Booth et al*., 2012; *Jaccard et al*., 2013; *Lamy et al*., 2014]. Dust deposition in the mouth of the Senegal River increased sharply with the onset of commercial agriculture in the Sahel region ~ 200 years ago [*Mulitza et al*., 2010], and paleodata suggest large increases in desert dust over much of the globe in the twentieth century [*Mahowald et al*., 2010]. Furthermore, satellite-based studies suggest substantial dust emissions due to land use perturbation, making future increases in desert dust likely [*Ginoux et al*., 2012; *Ward et al*., 2014]. Given that the overall radiative effect of dust in the atmosphere is likely negative and leading to cooling, increased dust concentrations in the atmosphere have the potential to mask future warming. However, studies on the effects of future climate change on dust loadings in the atmosphere give diverging results, resulting in an overall "low confidence" rating of climate change predictions of mineral dust in the recent Intergovernmental Panel on Climate

Change (IPCC) reports [*Boucher et al*., 2013]. Indeed, mineral dust and the uncertainties it introduces to our understanding of total aerosol radiative forcing and climate projections have been identified as critical research areas by the IPCC.

In addition to dust load (concentration) in the atmosphere, dust deposition is an important element of the dust cycle. However, direct measurements of dust deposition rates, in particular, over the open ocean, are currently scarce. The lack of observations is exacerbated by the fact that numerical model estimates of dust deposition vary greatly, especially over remote oceanic areas [*Schulz et al*., 2012; *Albani et al*., 2014]. Future evaluations and improvements of numerical models that quantify different features of the global dust cycle therefore require an adequate set of observations from the modern and past environment.

In marine sediments, ^{232}Th, a long-lived isotope of purely continental origin is often analyzed in conjunction with ^{230}Th, an isotope produced in seawater at a constant and well-known rate by decay of uranium-234 (^{234}U). Thorium is one of the most particle reactive elements in seawater and is quickly scavenged onto sinking particles and exported to the seafloor [*Bacon*, 1984; *Francois et al*., 2004, 2007]. Assuming that the flux of scavenged ^{230}Th to the seafloor is equal to its rate of production from ^{234}U-decay, there is a simple inverse relationship between the total flux of material accumulating on the seafloor and its concentration of scavenged ^{230}Th. This inverse relationship forms the basis of the ^{230}Th normalization method, which is increasingly considered to yield more accurate reconstructions of bulk particle fluxes to the seafloor than the traditional age model-based mass accumulation rate approach [e.g., *Francois et al*. 2004, 2007; *McGee et al*., 2010; *Marcantonio et al*., 2014]. To derive the ^{230}Th-normalized flux of a sedimentary component, the bulk flux is multiplied with the concentration of the variable of interest, i.e., ^{232}Th in this study.

Together, ^{232}Th and ^{230}Th thus offer a promising proxy to reconstruct dust deposition in the ocean over millennial and glacial-interglacial time scales. Indeed, this approach is increasingly used in paleoceanographic studies [*Adkins et al*., 2006; *Bradtmiller et al*., 2007; *Pourmand et al*., 2004; *Anderson et al*., 2006; *McGee et al*., 2007, 2013; *Winckler et al*., 2008; *Martinez-Garcia et al*., 2009; *Woodard et al*., 2012; *Kienast et al*., 2013; *Serno et al*., 2014; *Lamy et al*., 2014; *Jacobel et al*., 2016; *Costa et al*., 2016].

Here we compile Th data from the published literature from marine sediment cores and systematically explore the utility of ^{232}Th as a proxy for continental and dust inputs to the global ocean. The objective of this study is threefold. First, this work aims to increase the spatial coverage of ^{232}Th deposition records and to delineate the boundary between purely eolian and mixed continental inputs. Second, we combine the marine sediment data and results from climate modeling into a common framework to identify areas in which model-based and sediment based estimates of dust deposition are comparable. The focus is on the late Holocene (0–4 ka) time slice, but data for the Last Glacial Maximum (LGM, 19–23 ka) are also presented. Ultimately, the goal of this study is to provide observations from the past environment that will help to improve the predictive capabilities of the dust cycle component in global scale coupled models.

The paper is organized as follows. First, we summarize the background on the use of ^{232}Th as continental proxy and the underlying assumptions (section 2). The methodological approach (section 3) describes the assembly of the full database and the filters applied to exclude sites influenced by non-eolian continental material. In section 4, Th-based dust fluxes are presented for the 0–4 ka and the 19–23 ka time slices, and these estimates are compared with recent results from global coupled models (CCSM4 and CCSM3, *Albani et al*. [2014] and *Mahowald et al*. [2006], respectively).

2. Background

Thorium-232 is also known as primordial thorium because of its very long half-life (1.4×10^{10} years). Thorium-232 makes up almost all naturally occurring thorium in the Earth system, with other isotopes occurring only in trace amounts and as relatively short-lived decay products of the ^{238}U, ^{235}U, and ^{232}Th decay series. After ^{232}Th, ^{230}Th is the next most stable isotope with a half-life of 75,584 ± 110 years [*Cheng et al*., 2013]. We use ^{230}Th to normalize fluxes of ^{232}Th to the seafloor (section 1).

Thorium-232 is used as a dust proxy because its average concentration in upper continental crust (10.5–10.7 ppm) [*Taylor and McClennan*, 1985; *Rudnick and Gao*, 2004] (Figure 1) is roughly 50 times greater than that in mid-ocean ridge basalt (MORB)-like material (0.14–0.28 ppm) [*Klein*, 2004, *Kelemen et al*., 2004].

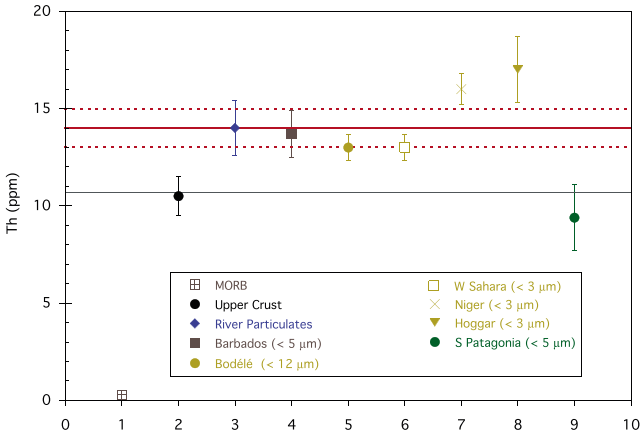

Figure 1. Th concentration in fresh mid-ocean ridge basalt (MORB, $n = 34$) [*Kelemen et al.*, 2004] compared to the composite value for upper crust based on extensive analysis of sediments and loess deposits [*Rudnick and Gao*, 2004). Black line indicates an earlier estimate of the average Th concentration in upper crust (10.7 ppm) [*Taylor and McClennan*, 1985], which has previously been used for dust reconstructions using ^{232}Th. Red line shows the recently recommended value (14 ± 1 ppm), which is the error weighted mean Th concentration in fine (<5 μm) samples from all global dust source areas except Patagonia [*McGee et al.*, 2016]. Th data from suspended particulates collected in the world's largest rivers systems ($n = 10$) are from *Martin and Meybeck* [1979]. Remaining points show Th concentrations in the fine fraction of African dust from Barbados (<5 μm, $n = 8$) [*Muhs et al.*, 2007], sediment and eolian deposits from the Bodélé Depression in Chad (<12 μm, $n = 1$), the western Sahara coastal region (<3 μm, $n = 1$), southwest Niger (<3 μm, $n = 1$), the Hoggar Massif in Algeria (<3 μm, $n = 1$; *all African data from Castillo et al.* [2008]), and from Patagonia (<5 μm, $n = 7$) [*McGee et al.*, 2016]. See supporting information Data Set S1 for details.

When the Earth's mantle is melted and magma forms, trace elements display a preference for either the melt phase (magma) or the solid phase, i.e., the minerals that crystallize from the magma as it slowly cools. The relatively large size (10^{-10} m) and high charge (+4) of thorium ions render them incompatible with mafic and intermediate minerals that crystallize early in the reaction series at relatively high temperatures. Instead, thorium is incorporated into felsic minerals, which are the last to crystallize when magma cools and which largely make up continental crust. The earlier crystallization of mafic and intermediate minerals progressively enriches the remaining magma in incompatible elements such as Th, explaining the large difference in concentration between upper continental crust and basaltic oceanic crust. In open ocean sediments, away from fluvial, hemipelagic, and glaciogenic inputs of continental material, any appreciable amounts of Th are therefore thought to have been delivered by an eolian pathway.

An implicit assumption underlying this approach is that thorium concentrations in upper continental crust, and materials derived from it such as mineral dust, are invariant and close to 10.7 ppm. This assumption has been largely confirmed in a compilation of various geologic materials < 63 μm [*McGee et al.*, 2007]. More recently, however, *McGee et al.* [2016] showed a systematic increase in Th concentrations with decreasing grain size in sediments from major dust source areas in East Asia, Australia, and central South America. In the <5 μm size range, the average Th concentration in these materials is 14 ± 1 ppm (Figure 1, red line), and this value is now recommended to estimate dust fluxes based on ^{232}Th where dust inputs are likely to be fine grained [*McGee et al.*, 2016]. The enrichment in fine size classes observed by *McGee et al.* [2016] is qualitatively supported by earlier Th measurements of global suspended (i.e., fine) river particulates in 10 of the world's largest river systems (14 ppm on average) [*Martin and Meybeck*, 1979] (Figure 1). Similarly, analysis of fine African dust collected on Barbados (13.7 ± 1.2 ppm) [*Muhs et al.*, 2007], fine sediment from the Bodélé Depression in Chad (13 ± 1.3 ppm) [*Castillo et al.*, 2008], and fine surface soil from the western Sahara (13 ± 1.3 ppm) [*Castillo et al.*, 2008] show Th concentrations close to 14 ppm (Figure 1 and Data Set S1 in the supporting information).

Some regional differences in dust composition, however, do exist (Figure 1). In fine dust (<3 μm) from the Hoggar region in Algeria, the Th concentration is 17 ± 1.7 ppm and reflects the more felsic and geochemically evolved nature of the igneous and metamorphic bedrock in the region [*Castillo et al.*, 2008; *Moreno et al.*, 2006]. Dust samples (<5 μm) from several coastal locations in Patagonia show Th concentrations close to $\sim 9.4 \pm 1.7$ ppm, likely due to the presence of basaltic to basaltic-andesitic volcanic bedrock [*McGee et al.*, 2016, *Gaiero et al.*, 2007].

On regional scales, the exact concentration of Th in mineral dust will depend on the bedrock geology, weathering history of the source region, the transport history, and dust grain-size [*Moreno et al.*, 2006; *Castillo et al.*, 2008; *McGee et al.*, 2016]. Acknowledging this caveat, the basic observation that ^{232}Th is significantly enriched

in continental versus ocean crust remains valid and enables the use of ^{232}Th as tracer of continental and dust input to the ocean. Given that atmospheric dust transported over long distances typically displays a fine and well-sorted grain-size distribution (2–5 μm)[e.g., *Prospero and Bonatti*, 1969; *Mahowald et al*., 2014, and references therein], we use 14 ppm instead of 10.7 ppm here as average ^{232}Th concentration in fine-grained continental material to quantify dust fluxes to the ocean.

The largest source of error in reconstructing dust flux using ^{232}Th in sediments is contamination by continental material of non-eolian origin, such as ice-rafted debris and hemipelagic material (i.e., terrestrial sediment that escaped the continental shelves). We systematically screen for these two sources of error by applying filters for latitude and distance offshore (section 3). Another potential bias is input of distal volcanic ash from regions of continental arc volcanism. For example, Quaternary ash tuff deposits in the northern Andes have relatively high Th concentrations (7.1 ppm ± 4.5 ppm, $n = 6$) [*Lebti et al*., 2006] and could lead to overestimating dust in the Eastern Equatorial Pacific (EEP). The delivery of ^{232}Th from continents leads to measurable concentrations (~pg/kg) of dissolved ^{232}Th ($^{232}Th_{diss}$) in seawater, which are increasingly used to quantify present day dust deposition [*Hsieh et al*., 2011; *Hayes et al*., 2013; *Lopez et al*., 2015]. The estimated fraction of dust-derived thorium that dissolves in seawater ranges from 1% to 20% [*Hsieh et al*., 2011; *Hayes et al*., 2013], and reabsorption of $^{232}Th_{diss}$ onto sinking particulates could lead to biases in low sedimentation rate regimes such as ocean gyres. Lastly, horizontal advection of fine particles by ocean surface currents can introduce uncertainties [*Siegel and Deuser*, 1997; *Bory et al*., 2002; *Han et al*., 2008], especially in fast flowing boundary currents [*Rühlemann and Butzin*, 2006, *van Sebille et al*., 2015].

3. Methods and Approach

3.1. Assembly of the Database

We compiled ^{232}Th, ^{230}Th, and ^{238}U sedimentary concentration data from the literature and from unpublished sources. We correct all ^{230}Th data for detrital and authigenic contributions and for decay since deposition based on established methods [*Henderson and Anderson*, 2003; *Francois et al*., 2004] and using the most recent half-life of ^{230}Th (75,548 ± 110 years) [*Cheng et al*., 2013]. Corrections for detrital ^{230}Th were applied using ^{238}U/^{232}Th activity ratios suggested for the Atlantic (0.6), Pacific (0.7), and Southern Ocean (0.4) following *Henderson and Anderson* [2003]. For the Arabian Sea, 0.6 was used. We adopt core chronologies from the original publications, and we include U/Th data sets here that have not been used as dust indicators in their original contexts. References to the original studies are given in the supporting information. We multiply the ^{230}Th-normalized bulk flux with the concentration of ^{232}Th to derive normalized ^{232}Th-fluxes with an average uncertainty (2 sigma) of 10%. The above approach is taken for all data sets with two exceptions. In two recent studies from the subarctic North Pacifc [*Serno et al*., 2014] and off subtropical Africa [*McGee et al*., 2013], geochemical and grain size corrections were applied to the ^{232}Th data to derive a refined estimate of dust deposition (see below). In these cases, we do not perform any recalculations here but take the dust fluxes directly from the original studies

3.2. Description of the Full Database

The database contains records ($n > 300$) from all major ocean basins and includes sites from polar, temperate, and tropical regions. However, not all sites are suitable for dust reconstructions, as marine sediments typically are mixtures of various components. The lithogenic component, which includes not only continental dust but also ice rafted debris and hemipelagic material forms the largest sediment input term to the ocean (20 Gigatons/yr), followed by biogenic debris (2 Gigatons/yr), volcanic ash, authigenic minerals, and meteoritic debris. Reliable dust reconstructions based on marine sediment cores therefore require careful site selection [*Kohfeld and Harrison*, 2001]. We do not expect meteoritic and authigenic inputs to bias our ^{232}Th-based dust estimates due to their negligible overall magnitude. The largest potential bias to our estimates comes from hemipelagic and ice rafted contributions, both of which deliver significant amounts of continental ^{232}Th that is not associated with dust.

3.3. Screening of the Database

3.3.1. Identifying Hemipelagic Sites

Figures 2a and 3a show late Holocene (0–4 ka) Th-normalized ^{232}Th fluxes for all sites plotted against distance offshore and latitude, respectively. Many high values are found within 300 km off the coast, where fluvial and

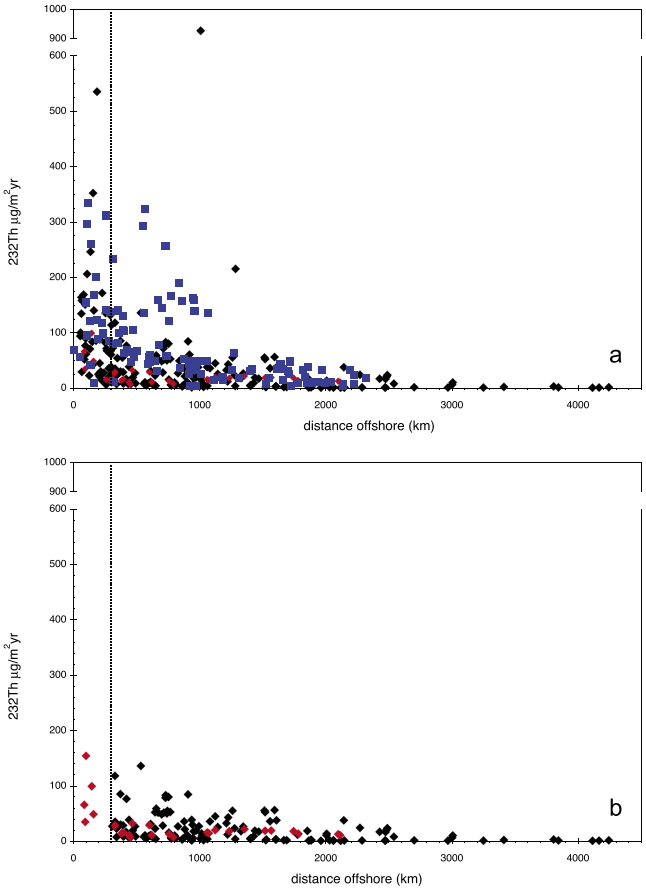

Figure 2. Thorium-232 fluxes (0–4 ka) plotted against distance offshore for the (a) full and (b) screened database in units of $\mu g/m^2$ yr. Sites from latitudes more polar than 50° (Southern Ocean and North Atlantic) and 55° (North Pacific) are in shown in blue squares; sites for which corrections have been applied to isolate the eolian signal from other continental inputs in the original references are in red. Note gap in *y* axis. See supporting information for data sources.

hemipelagic inputs are likely to be important. Beyond 300 km from the coast, most sites of nonpolar origin (Figure 2a, black and red symbols) have ^{232}Th flux values $<200\,\mu g/m^2yr$ and fluxes further decrease with increasing distance offshore. Similar to our findings, *Singh et al*. [2011] observed that Holocene ^{232}Th fluxes drop off precipitously with increasing distance from shore in the EEP. In order to avoid hemipelagic contributions, we categorically exclude all core sites that are within 300 km from the coast prior to reconstructing dust fluxes. Given significant fluvial inputs of the Amazon River [e.g., *Francois and Bacon*, 1991], the cutoff is 600 km and 800 km during the 0–4 ka and 19–23 ka time slice, respectively, in the western tropical Atlantic. Off subtropical Africa, however, *McGee et al*. [2013] combined grain-size end-member modeling and ^{230}Th-normalized bulk fluxes to correct for fluvial/hemipelagic inputs and to isolate the eolian signal in a set of cores that cover the last 20 ka. The 300 km offshore criterion is thus not applied in this data set (Figures 2a and 2b, red symbols). A second data set in which corrections have been applied is from *Serno et al*. [2014], who used ^{4}He and ^{232}Th measurements in fine ($<8\,\mu m$) Asian dust source samples and a mixing model to isolate the eolian ^{232}Th component in a large set of core top samples from the subarctic North Pacific (Figures 2a and 2b, red symbols).

3.3.2. Identifying Sites Affected by Ice Rafted Debris

A steep poleward increase in fluxes is evident between 55–70°N and 55–70°S in the unscreened database (Figure 3a), likely as result of ice rafting around the Arctic and Antarctic continental margins. Under modern conditions, large tabular icebergs originating from the Antarctic ice sheet initially accumulate in the Weddell Sea and then travel northward until approximately 60°S, where they are swept into the eastward flowing Antarctic Circumpolar Current (ACC) [*Stuart and Long*, 2011]. Most icebergs have broken up by the time they reach the ACC [*Stuart and Long*, 2011] and are thus unlikely to occur in large numbers north of 50°S. To avoid ice-rafted debris, we categorically exclude all sites more polar than 50° prior to reconstructing dust fluxes in the Southern Ocean and North Atlantic. Given the absence of a large continental ice sheet, the cutoff is only 55° in the North Pacific. We apply the same cutoff in the glacial time slice (19–23 ka, supporting information Figures S1 and S2), even though there is paleoevidence that the Antarctic Polar Front may have shifted northward by 3–5° latitude [*Kohfeld et al*., 2013, *Kanfoush et al*., 2000]. Nevertheless, the glacial database does not show a steep increase between 55 and 70°N and 55 and 70°S, possibly because it contains much fewer sites. Acknowledging that the cutoffs used here are fixed in space and time, and thus static with climate, we think that the lack of direct observational constraints, including from particle size distributions and source fingerprinting, renders the isolation of ice-rafted debris inputs at all sites hard to conclusively evaluate at this time.

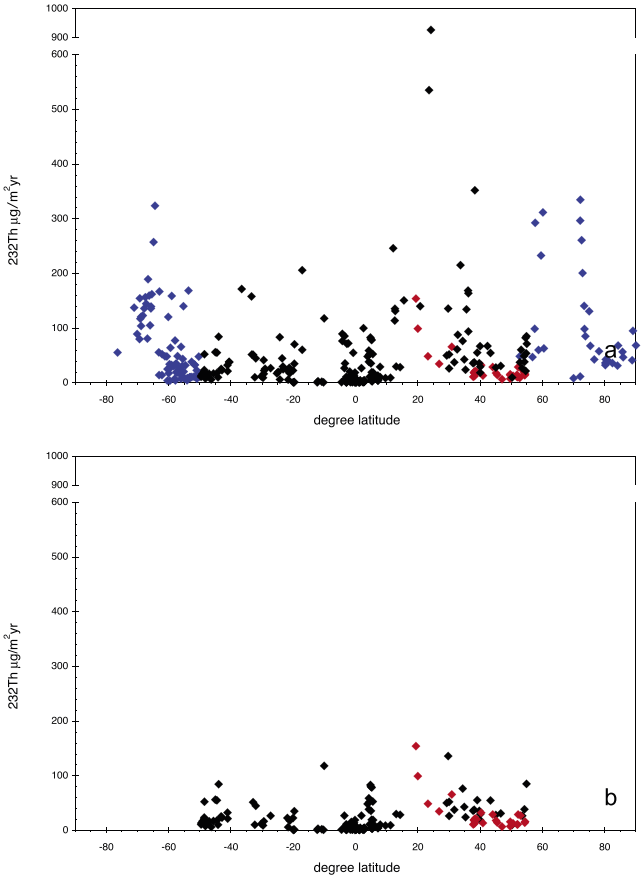

Figure 3. Thorium-232 fluxes (0–4 ka) plotted against latitude for the (a) full and (b) screened database in units of $\mu g/m^2$ yr. See Figure 2 for symbol colors.

In addition to the latitudinal and distance-offshore filters, we also screen out sites that are known drift deposits, those without chronological control, and sites affected by fluvial inputs even though they are beyond 300 km offshore. Figures 2b and 3b display ^{232}Th fluxes in the 0–4 ka time slice for the screened database versus distance offshore and latitude, respectively (see supporting information Figures S1 and S2 for 19–23 ka time slice).

3.3.3. Dust Deposition in ThoroMap

In the following, we use the screened database to derive dust deposition by dividing ^{230}Th-normalized fluxes of ^{232}Th by 14 ppm and refer to it as ThoroMap. The average analytical error of ^{232}Th-fluxes (±10%) and the reported uncertainty around the fine-grained crustal average (±1 ppm) [*McGee et al*., 2016] would result in a combined error of 12%. However, acknowledging regional differences in ^{232}Th concentration of fine-grained material, we take the difference between the recommended global value (14 ppm) and the Patagonian average (9.4 pm) to derive an uncertainty of ± 4.6 ppm around the fine-grained crustal average. This leads to a more conservative combined error of ±35%. The quantification of other potential sources of error, such as surface advection of suspended particles, is beyond the scope of the present study but could be investigated using circulation models in the future [e.g., *Rühlemann and Butzin*, 2006; *van Sebille et al*., 2015]. ThoroMap contains 157 and 76 sites in the 0–4 ka and 19–23 ka time slice, respectively. References to the original data sources are given in supporting information Data Sets S2 and S3.

3.4. Models Used

ThoroMap is compared with output from two numerical models. The most recent one is the Community Atmosphere Model version 4 (CAM4) [*Albani et al*., 2014], which is part of the new Community Climate System Model CCSM4. CCSM4 and its predecessor CCSM3 [*Mahowald et al*., 2006] are coupled atmosphere, land, ocean and sea ice models used for climate change scenarios [e.g., *Hurrell et al*., 2013]. In CCSM3, *Mahowald et al*. [2006] introduced a mineral aerosol source and deposition algorithm [*Zender et al*., 2003] to parameterize the sources, transport, and deposition of mineral dust. Sources of dust were assumed to be dry, unvegetated regions with strong winds. Deposition processes include dry gravitational settling, turbulent dry deposition, and wet deposition during precipitation. The source and deposition schemes were slightly modified between CAM3 and CAM4, mostly due to a shift in the assumed size distribution to larger sizes (*Albani et al*. [2014]; following *Kok* [2011]). Also, wet deposition in CAM4 was changed by increasing the solubility for dust particles and by using a larger below cloud scavenging coefficient for larger particles. Note that for CCSM4, we specifically use a 2 ka simulation (C4fn_2k) [*Albani et al*., 2015] to make comparisons with the 0–4 ka time slice presented here. For CCSM3, no 2 ka simulation is available, and we use the simulation for the current climate (CCSM3 SMOB) [*Mahowald et al*., 2006]. Both CCSM4 and CCSM3 have published simulations for the LGM, which are used here to make comparisons with the 19–23 ka ThoroMap time slice.

Table 1. Model Runs and Statistical Correlations (Spearman's Rho) to ThoroMap in the 0–4 ka and 19–23 ka Time Slice[a]

Model	Scenario	Time	Model Reference	Sites	Rho
CCSM4	Cf4n_2k	2 ka	*Albani et al.* [2015]	135 (157)	0.59
CCSM3	SMOB	Current	*Mahowald et al.* [2006]	148 (157)	0.63
CCSM4	Cf4n_lgm	19–23 ka	*Albani et al.* [2014]	54 (76)	0.83
CCSM3	SMOB_lgm	19–23 ka	*Mahowald et al.* [2006]	67 (76)	0.82

[a]Sites included in the correlation do not include any sites that have previously been used to tune the models. The numbers of all screened sites in ThoroMap is given in brackets.

ThoroMap includes a limited number of sites that are also contained in the original data sets used to tune CCSM3 (DIRTMAP) [*Kohfeld and Harrison*, 2001] and CCSM4 (supporting information Table S3 [*Albani et al.*, 2014] and Table 1 [*Albani et al.*, 2015]), respectively. We exclude all of them prior to calculating correlation factors between models and Th-based dust (Figures 7 and 8 and Table 1), irrespective of the methods used to derive dust fluxes in the original publications.

4. Dust Reconstructions Based On ThoroMap

4.1. The Late Holocene Time Slice

In the late Holocene, Th-based dust fluxes ($n = 157$) range from roughly 0.1 to 17.7 g/m^2 yr (Figure 4a). Minimum deposition rates are observed in the eastern and western equatorial Pacific (EEP and WEP, respectively) and the Pacific sector of the Southern Ocean. Thorium-based dust fluxes are maximal off northwest Africa, consistent with the proximity of this region to the Sahara-Sahel dust corridor. Relatively high values are also found at one site off Florida (9.7 g/m^2 yr). It is surprising to only have a slightly lower deposition flux ~500 km off Florida compared to Africa, as changes in dust size distribution indicate scavenging (i.e., dry or wet deposition) [*Maring et al.*, 2003; *Mahowald et al.*, 2014] and dust deposition observed in Miami, Florida from 1982–1983, was 1.6 g/m^{2}yr [*Prospero et al.*, 1987]. Possible explanations include that (a) there are significant variations of the seasonal positioning of the African dust plumes or (b) that this feature results from the vertical level of dust transport and the different scavenging mechanisms close to the African coast (prevalently dry) compared to the Caribbean (prevalently wet). Alternatively, the site off Florida could be biased by sediment redistribution in the strong nepheloid layer observed in this region [*McCave*, 1986], which may have biased the deposition flux despite Th-normalization. Unfortunately, a current lack of detailed observations (including on dust size and scavenging) prevents reaching any firm conclusion on this aspect.

Deposition rates are moderately high in the subarctic North Pacific (1–4 g/m^2 yr) and in the tropical Atlantic off Brazil (4–6 g/m^2 yr). ThoroMap also suggests moderately high deposition rates in the Atlantic sector of the Southern Ocean, where dust deposition decreases from 2–6 g/m^2 yr off Argentina to 0.5–2 g/m^2 yr farther east. All sites are north of the Polar Front, rendering ice-rafted inputs unlikely.

4.2. The 19–23 ka Time Slice

During the LGM, Th-based dust deposition rates ($n = 76$) range from 0.1 to 29 g/m^2 yr (Figure 4b). Dust fluxes are higher than during the late Holocene at all sites, except off subtropical northwest Africa (Figure 4c). Sites in the North Atlantic show deposition rates between 10 and 29 g/m^2 yr, a two- to threefold increase over late Holocene rates. Dust deposition is also strongly increased in the subarctic North Pacific and in the Atlantic sector of the Southern Ocean. In the EEP and WEP, glacial dust fluxes are consistently 2–3 times higher than late Holocene ones. Averaging from 0 to 7 ka instead of 0–4 ka, there is a two- to threefold glacial increase in dust deposition supported by additional sites in the Indian Sector of the Southern Ocean (not shown).

ThoroMap shows increased dust deposition during the LGM compared to the late Holocene in all three of the modern HNLC regions, i.e., the Southern Ocean, the subarctic Pacific, and the EEP. Earlier studies using age-model-based mass accumulation rates of operationally defined eolian material found increased dust deposition during interglacials in the EEP [*Rea*, 1994; *Murray et al.*, 1995]. However, more recent studies using Th-normalized fluxes of ^{232}Th show that dust deposition was enhanced during glacials in the EEP and WEP [*Anderson et al.*, 2006; *McGee et al.*, 2007; *Winckler et al.*, 2008; *Kienast et al.*, 2013; *Winckler et al.*, 2016; *Jacobel et al.*, 2016; *Costa et al.*, 2016]. Based on a significant number of additional sites, ThoroMap supports these findings.

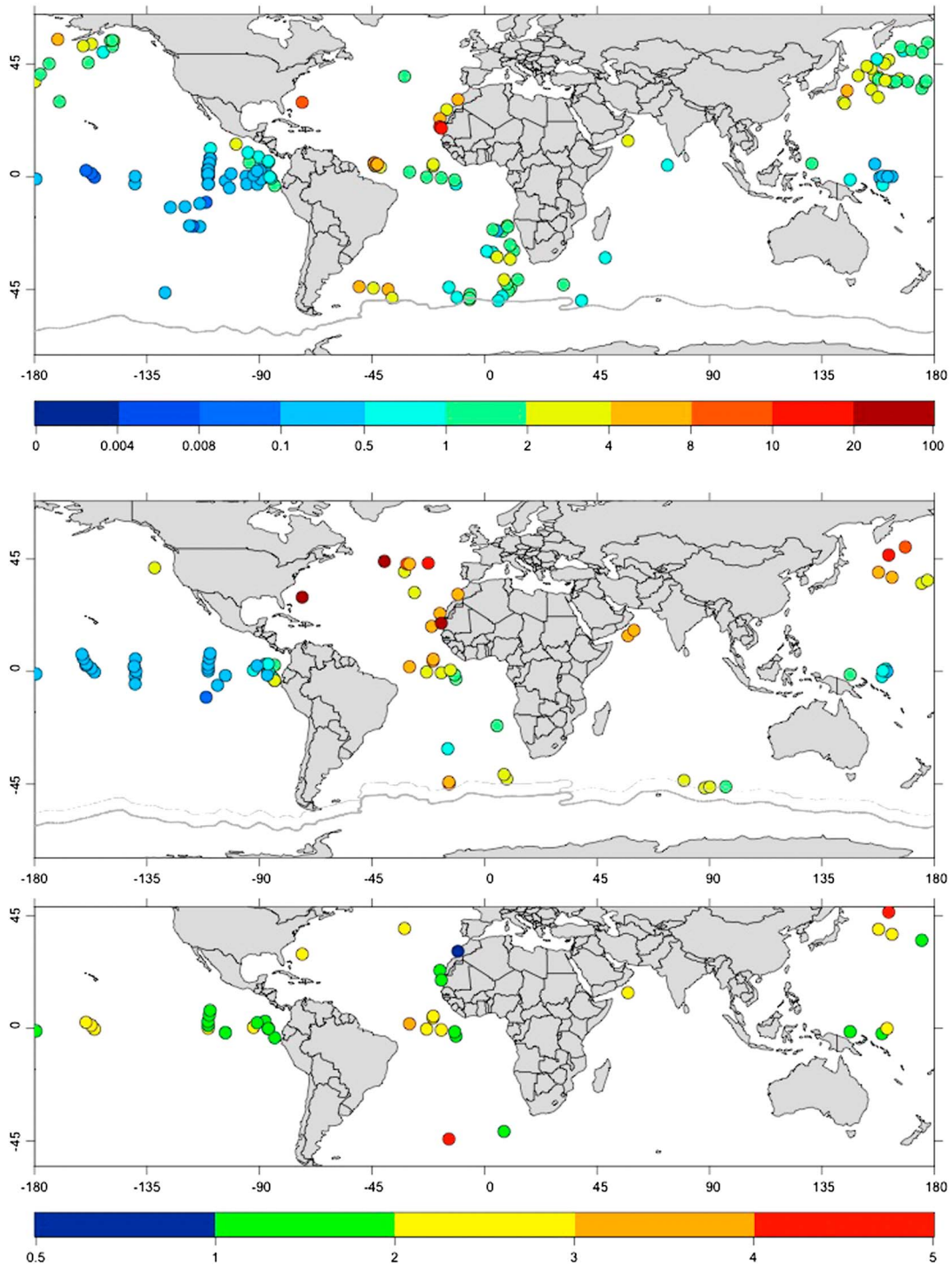

Figure 4. ThoroMap dust deposition (g/m^2 yr) in the (top) late Holocene (0–4 ka) and the (middle) LGM (19–23 ka). Note nonlinear color bar. The position of the modern Polar Front [*Orsi et al*., 1995] is indicated in grey (Figure 4, top and middle) and has been shifted north by 5° (Figure 4, middle). (bottom) LGM/late Holocene ratios.

4.3. Comparison to Other Data Sets

DIRTMAP is an earlier global compilation of dust fluxes based on terrestrial loess deposits, ice cores, marine sediment traps, and marine cores [*Kohfeld and Harrison*, 2001; *Kohfeld*, 2002; *Maher et al*., 2010]. In Figure 5, we compare ThoroMap (top) with Holocene dust flux estimates from DIRTMAP-2 (middle). While the number and locations of sites are different in the two data sets, which makes direct comparisons difficult, the two data

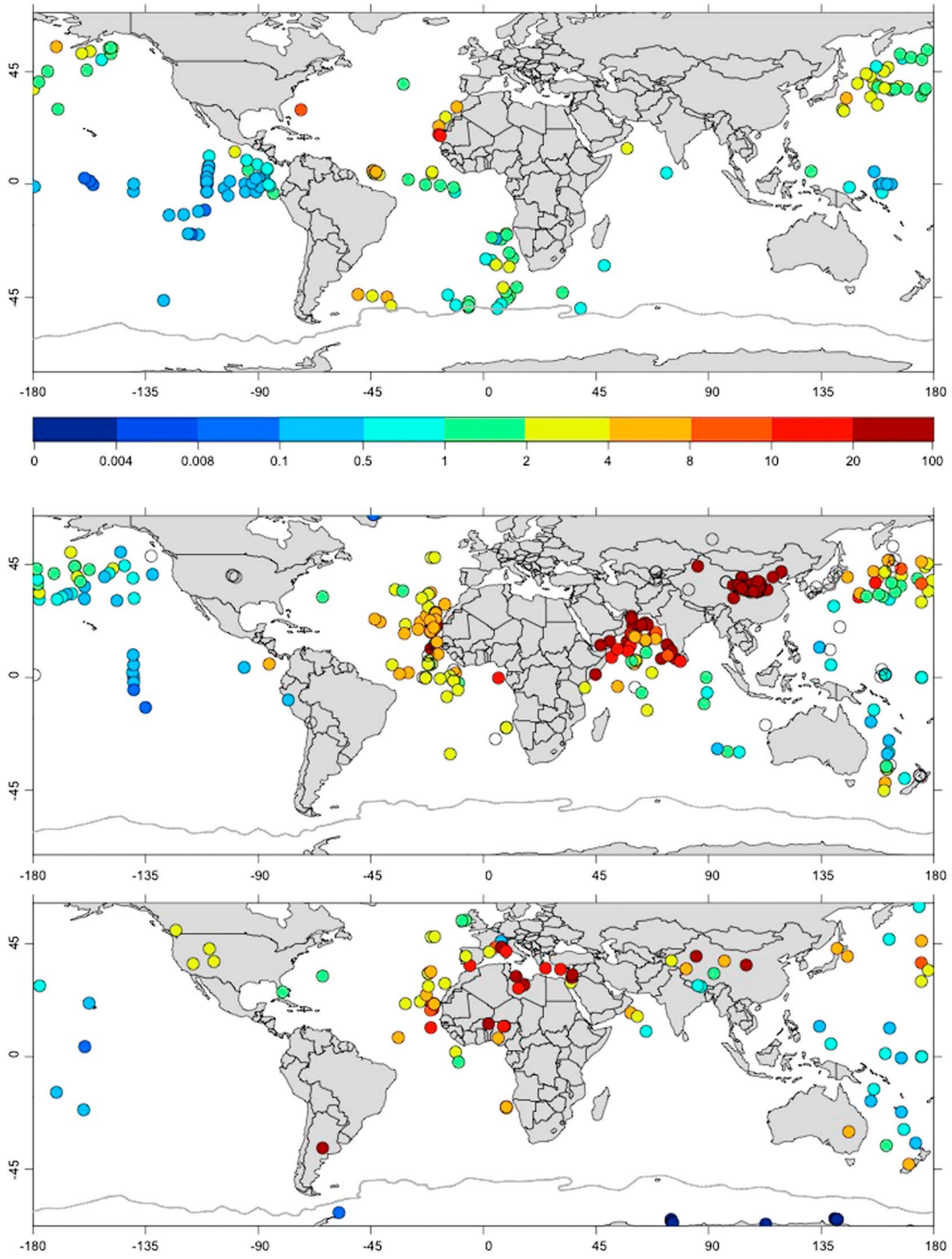

Figure 5. ThoroMap dust deposition (g/m^2 yr) for the (top) late Holocene (0–4 ka) compared to (middle) DIRTMAP-2 (0–10 ka) [*Kohfeld*, 2002] and the observational database of modern dust deposition (≤10 μm) by *Albani et al.* [2014]. The position of the modern Polar Front [*Orsi et al.*, 1995] is indicated in grey.

sets compare favorably overall. This is particularly true for the equatorial regions. However, ThoroMap differs from earlier dust flux reconstructions based on marine sediment cores, such as those compiled in DIRTMAP, in two key aspects. The earlier compilations are based on accumulation rates of the eolian fraction in sediments, where (a) accumulation rate is the product of the age-model based linear sediment rate and dry bulk density (standard deviation error ±10–25%) and (b) the eolian fraction is typically only operationally defined.

This means that the sediment is subjected to various chemical leaching steps to isolate a crystalline, inorganic residue that is assumed to be eolian. The standard error with estimating the eolian fraction in this way is reported as ±10–40% in DIRTMAP [*Kohfeld*, 2002]. In this approach, the eolian fraction cannot be distinguished from other lithogenic fractions such as volcanic ash or ice rafted debris [*Olivarez et al*., 1991; *Serno et al*., 2014], which can lead to erroneously high estimates. Furthermore, it is now well recognized that age-model based accumulation rates cannot distinguish between laterally advected particle fluxes and vertical particle fluxes from the sea surface, which are the variable of interest [e.g., *Francois et al*. 2004, 2007; *Kienast et al*., 2007; *Marcantonio et al*., 2014]. ThoroMap makes use of the increased availability of inductively coupled plasma–mass spectrometry (ICP-MS) measurements of Th and U isotopes and thus offers two important advantages. The eolian fraction is measured more directly with ^{232}Th, and flux estimates based on ^{230}Th-normalization are significantly less likely to be biased by local-scale syndepositional sediment redistribution on the seafloor compared to traditional age-model based chronologies. Thorium normalization also reduces sensitivity to age-model errors.

Recently, *Albani et al*. [2014] compiled modern dust flux observations from atmospheric sampling, ice cores, and sediment traps and included an estimate of the $<10\,\mu$m fraction (Figure 5, bottom). This data set also compares well with ThoroMap, in particular in the WEP and off northwest Africa. Note that the dust values observed off Argentina (2–6 g/m^2 yr) in ThoroMap (Figure 5a) fall on a gradient between values of >20 g/m^2 yr in continental Argentina and <0.1 g/m^2 yr on James Ross Island, Antarctica (Figure 5c).

4.4. Comparison Between ThoroMap and Models

In an ideal comparison between geological observations and models, particle size ranges would coincide. While CCSM4 simulates dust diameters $\leq 10\,\mu$m, ThoroMap does not presently include specific size information. Given that the inverse relationship between grain size and distance from source area is widely recognized [*Albani et al*., 2015; *Lawrence and Neff*, 2009; *Pye*, 1995, *Prospero and Bonatti*, 1969], we assume here that dust reaching screened sites in ThoroMap is predominately fine ($<10\,\mu$m) and that the following comparisons are robust.

4.4.1. Late Holocene

ThoroMap offers insight in areas such as the Atlantic sector of the Southern Ocean and the EEP, which are not well represented in current observational databases (Figure 5). After excluding any sites that have been used in the calibration of the models (section 3.5), we directly compare the model output with ThoroMap (Figures 7 and 8). The range in absolute dust values (0–4 ka) is remarkably similar between ThoroMap (0.08–9.73 g/m^2 yr, $n = 135$) and CCSM4 (0.02–7.96 g/m^2 yr). Model-data agreement is within a factor of 10 at many sites with a statistical correlation of 0.63 for CCSM3 and 0.59 for CCSM4 (Table 1) in the late Holocene time slice.

At none of the sites do the models overestimate dust deposition by more than a factor of 10; however, they underestimate it by a factor of 10 or more in some locations in comparison to ThoroMap. The number of apparently underestimated sites in CCSM4 is greater than in CCSM3 (Figure 7). CCSM4 predicts lower late Holocene dust deposition in comparison to ThoroMap chiefly in the Atlantic sector of the Southern Ocean (off Argentina) and the midlatitude South Atlantic (Figures 6 and 7a, light blue circles and open purple squares). Interestingly, the agreement between ThoroMap and the earlier CCSM3 model is much higher in these two regions (Figure 7b). In addition, CCSM4 and CCSM3 predict much lower dust fluxes than ThoroMap in the WEP (Figures 6 and 7a and 7b, solid red squares).

ThoroMap sites in the Atlantic sector of the Southern Ocean could, in principle, be contaminated by unrecognized ice-rafted inputs north of the Polar Front, although we consider systematic contamination by ice-rafted debris north of 50°S unlikely (section 2). Note that using ~ 9.4 instead of 14 ppm as a regional crustal Th-concentration for South America (section 2) would make the Th-based dust estimates even higher in this region. This area is subject to strong bottom currents [*McCave*, 1986], which could lead to errors in estimating sedimentary fluxes even when using Th normalization. However, the model-data agreement in this region is much better for CCSM3, consistent with the difficulty of the CCSM4 model to obtain realistic dust sources in South America without tuning [*Albani et al*., 2014]. Also, observed modern dust deposition is high in Argentina (>20 g/m^2 yr, Figure 5, bottom), in line with ThoroMap estimates offshore of South America. A 6 ka simulation [*Albani et al*., 2015] is in better agreement with the late Holocene time slice in ThoroMap in

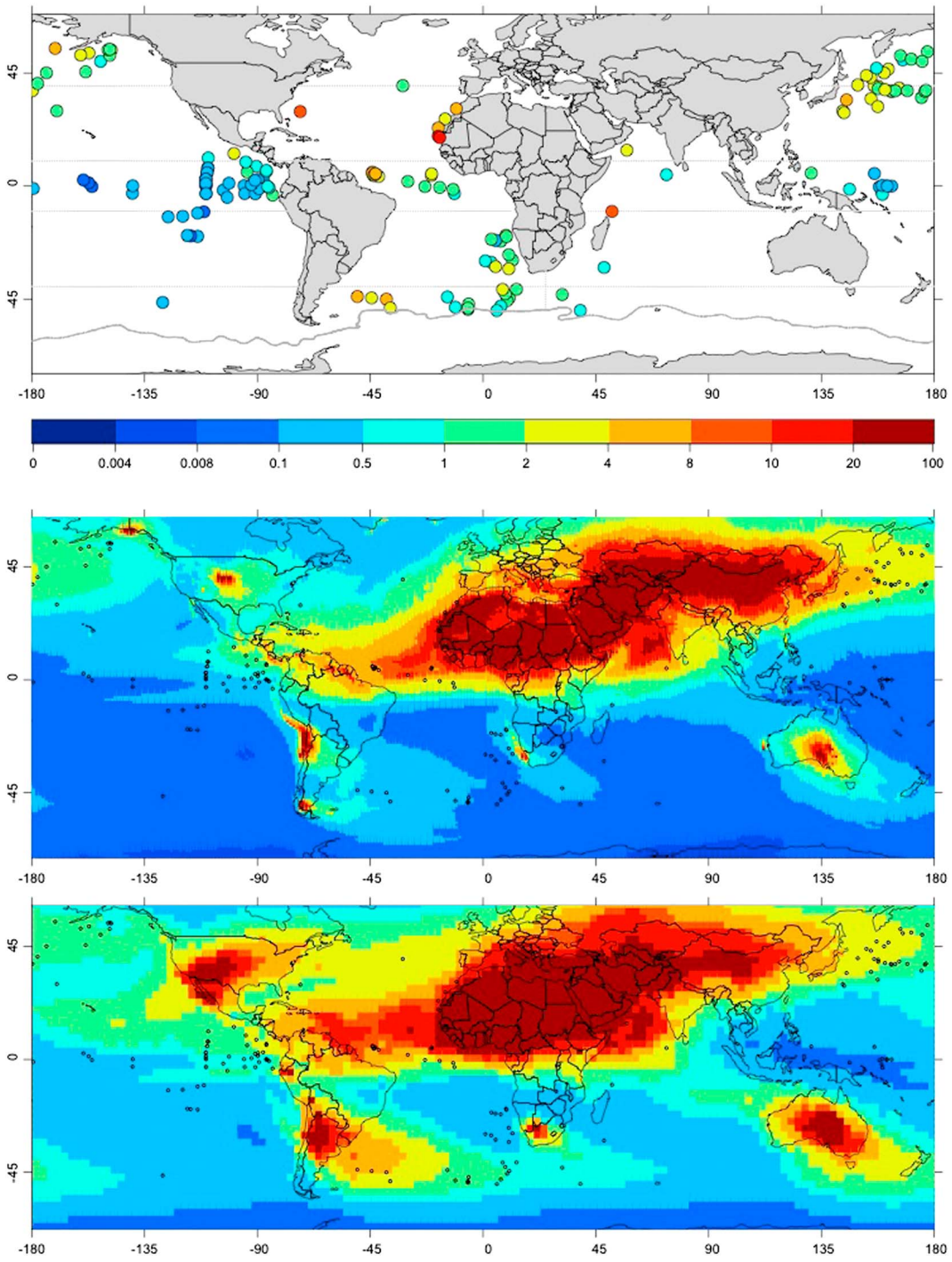

Figure 6. ThoroMap dust deposition (g/m^2 yr) for the (top) late Holocene (0–4 ka) compared to (middle) CCSM4 (case C4fn_2k) and (bottom) CCSM3 (case SMOB). Note nonlinear color bar. The position of the modern Polar Front [*Orsi et al.*, 1995] is indicated in grey (Figure 6, top). Zonal grey lines (Figure 6, top) delineate the regions discussed in text and Figure 7 and 8.

the Atlantic sector of the Southern Ocean, suggesting that some of the discrepancy between CCSM4 and ThoroMap could be related to the choice of time interval.

In the subarctic and midlatitude Pacific, the match between both models and ThoroMap is good (Figures 6, 7a and 7b, dark blue and green squares and circles). Similarly, the correlation between both models, in

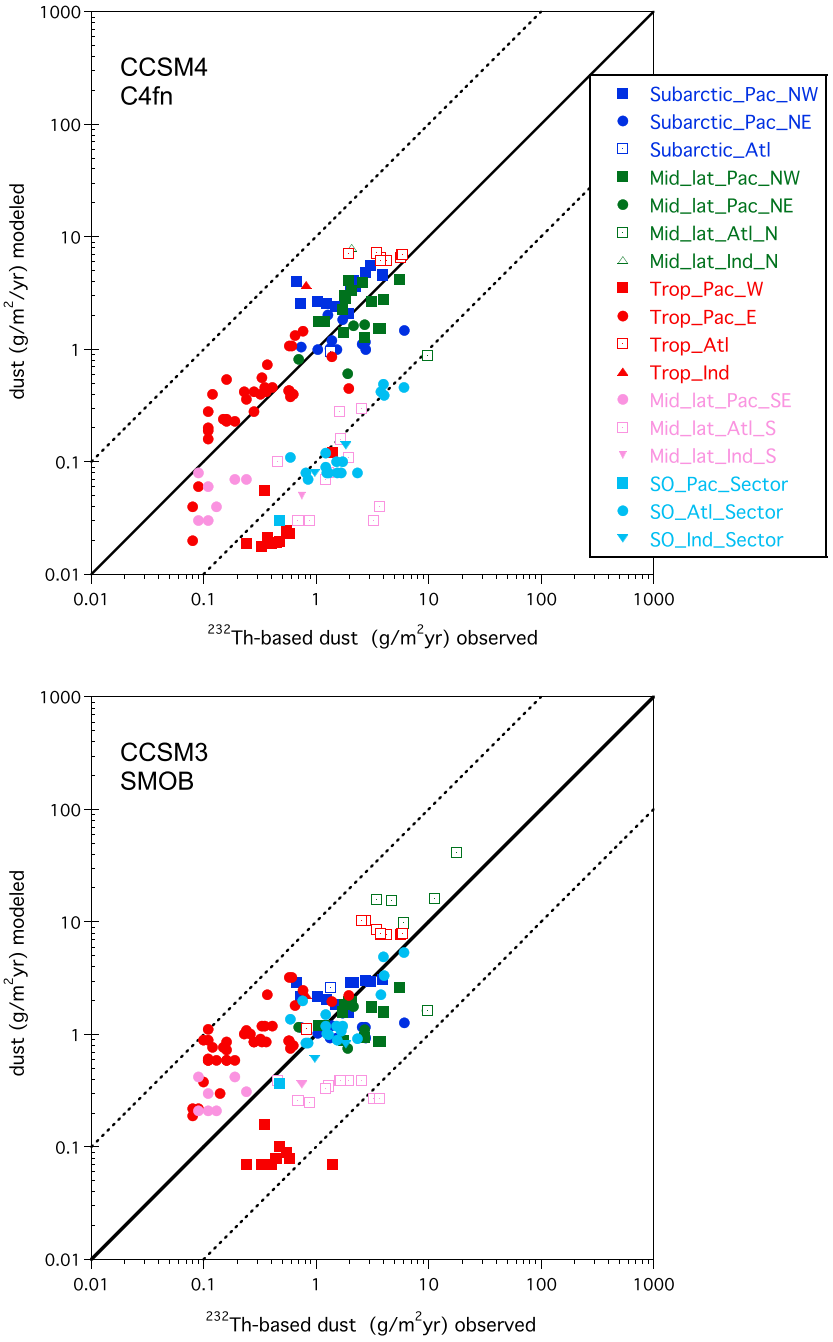

Figure 7. ThoroMap (0–4 ka) plotted against (top) CCSM4 and (bottom) CCSM3. Symbols are color coded according to latitude and ocean basin (see lines in Figure 6, top). Subarctic sites originate from 40 to 50°N in the Atlantic and 40–55°N in the Pacific. Midlatitude sites originate from 40 to 10°N and 40 to 10°S, tropical sites are from 10°S to 10°N, Southern Ocean sites originate from 40 to 50°S. Sites that have used previously to tune the models are excluded.

particular, CCSM4, and ThoroMap is strong in the EEP (Figures 6, 7a and 7b, red circles). However, both models appear to underestimate dust deposition in the WEP, CCSM4 even more so than CCSM3 (Figures 7a and 7b; red squares). An earlier, composite model [*Mahowald et al*., 2005] (not shown) predicts deposition rates of ~0.1–0.5 g/m^2 yr in the WEP and would thus fit better with ThoroMap in this region. This observation, in agreement with *Winckler et al*. [2008], suggests that dust sources may be underestimated in the WEP by both CCSM4 and CCSM3.

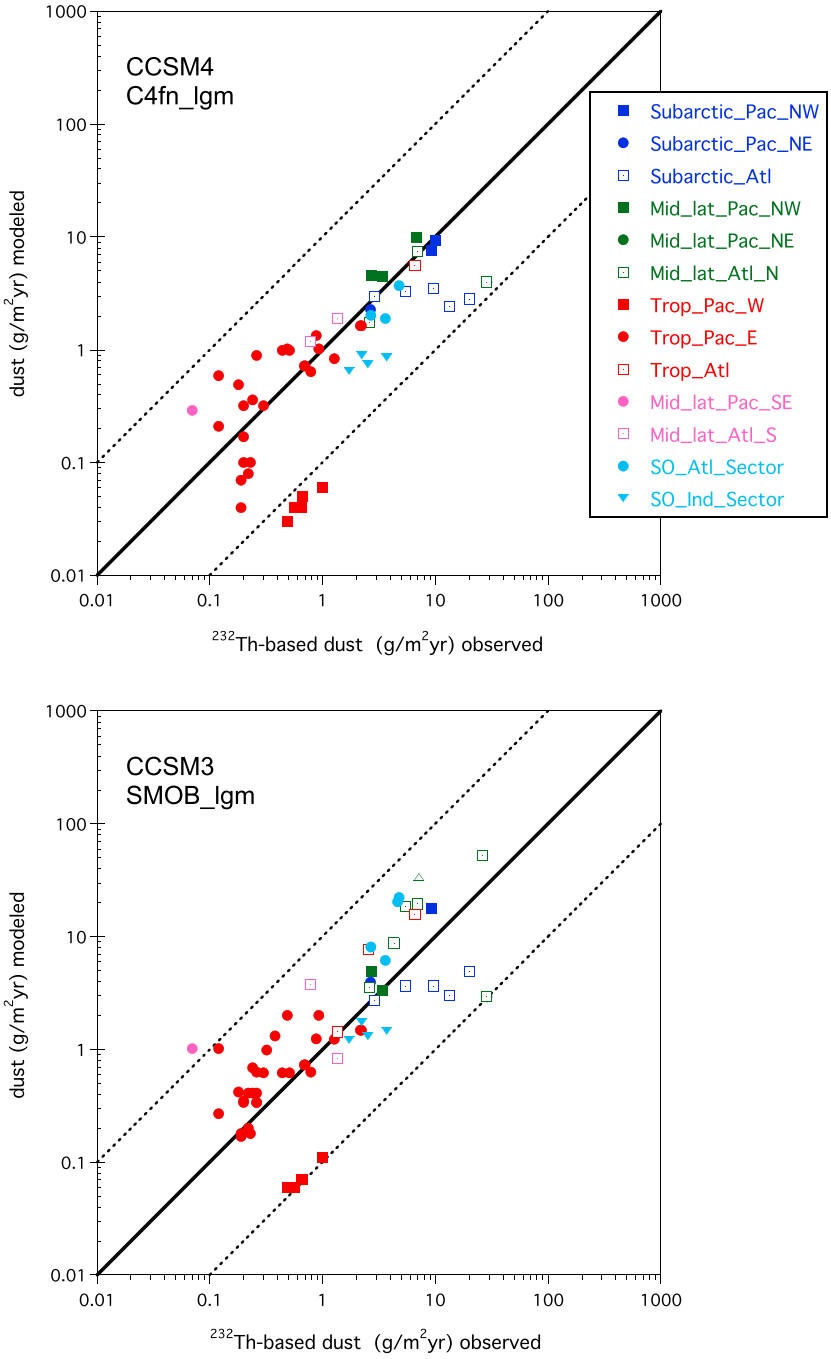

Figure 8. ThoroMap (19–23 ka) plotted against (top) CCSM4 and (bottom) CCSM3. Symbols are color coded according to latitude and ocean basin (see lines in Figure 6 (top) and Figure 7 caption). Sites that have been used previously to tune the models are excluded.

4.4.2. The 19–23 ka Time Slice

The statistical correlation between ThoroMap and models is high for the 19–23 ka time slice, with a Spearman's rho of 0.83 for CCSM4 ($n = 54$) and 0.82 for CCSM3 ($n = 67$; Table 1). The WEP is the only region where both models underestimate dust flux by a factor of 10 compared to ThoroMap (Figures 8a and 8b; solid red squares).

5. Conclusions

We compiled published ^{232}Th, ^{230}Th, and ^{238}U data and chronological information from marine sediment cores to build ThoroMap, a new global database of marine dust deposition records for the late Holocene (0–4 ka) and the LGM (19–23 ka). ThoroMap is compared to output from two recent coupled climate models, CCSM3, and CCSM4. Key findings are as follows:

1. Th-based dust fluxes range from 0.1 to 17.7 g/m^2 yr during the late Holocene ($n = 157$) with minimal deposition in the EEP, WEP, and the Pacific sector of the Southern Ocean. Maximum dust fluxes are observed off northwest Africa, consistent with the proximity of this region to the Sahara-Sahel dust source region.
2. As in previous studies, late Holocene dust fluxes are significantly lower than LGM fluxes, which range from 0.1 to 29 g/m^2 yr ($n = 76$). The only exception is off northwest Africa, downstream of the Sahara-Sahel dust corridor, where glacial and late Holocene dust fluxes are not significantly different.
3. Th-based dust deposition in the WEP is significantly higher than predicted by both CCSM3 and CCSM4 in the late Holocene as well as the LGM.
4. The observed match between CCSM4 and ThoroMap is good in the EEP, the subarctic and midlatitude Pacific, and off northwest Africa in the late Holocene. CCSM3 agrees with ThoroMap in these regions as well as in the Atlantic sector of the Southern Ocean. In the 0–4 ka time slice, data-model correlation factors are 0.59 and 0.63 for CCSM4 ($n = 135$) and CCSM3 ($n = 148$), respectively. In the LGM time slice, the match between models and Thoromap is 0.82 (CCSM4, $n = 54$) and 0.83 (CCSM3, $n = 67$). All sites included in these correlations have not been used previously to tune the models.
5. ThoroMap builds on DIRTMAP, an earlier widely used global compilation of dust deposition. Making use of the increased availability of ICP-MS measurements, ThoroMap exclusively uses ^{230}Th-normalized fluxes of the continental isotope ^{232}Th to estimate dust deposition, with an estimated uncertainty of 35%. Thus, ThoroMap is able to refine DIRTMAP in two important aspects. The eolian fraction is measured more directly with ^{232}Th, and accumulation is more accurately estimated by ^{230}Th normalization.

Acknowledgments

We greatly acknowledge official reviews by David McGee and one anonymous reviewer, which improved the manuscript, and fruitful discussions with Karen Kohfeld, Dan Kelley, Anne Marie Ryan, and Bob Anderson. Roger François and Samuel Jaccard generously shared unpublished data. S.K. was supported by grants from the National Science and Engineering Council Canada (NSERC). J.L. was supported by the FP7-PEOPLE-2013-IEF, Marie Curie proposal 622483. G.W., N.M., and S.A. were supported by the US National Science Foundation, through grants AGS-1003505 and 1003509. ThoroMap contributes to the goals of the Past Global Changes (PAGES) working group DICE (Dust Impacts on Climate and Environment) and will be made available as supporting information to this article and at NOAA NCEI, https://www.ncdc.noaa.gov/data-access/paleoclimatology-data.

References

Adkins, J., P. deMenocal, and G. Eshel (2006), The "African humid period" and the record of marine upwelling from excess Th-230 in Ocean Drilling Program Hole 658C, *Paleoceanography*, *21*, PA4203, doi:10.1029/2005PA001200.

Albani, S., N. M. Mahowald, A. T. Perry, R. A. Scanza, C. S. Zender, N. G. Heavens, V. Maggi, J. F. Kok, and B. L. Otto-Bliesner (2014), Improved dust representation in the Community Atmosphere Model, *J. Adv. Model. Earth Syst.*, *6*, 541–570, doi:10.1002/2013ms000279.

Albani, S., et al. (2015), Twelve thousand years of dust: The Holocene global dust cycle constrained by natural archives, *Clim. Past*, *11*(6), 869–903, doi:10.5194/cp-11-869-2015.

Anderson, R. F., M. Q. Fleischer, and Y. Lao (2006), Glacial-interglacial variability in the delivery of dust to the central equatorial Pacific, *Earth Planet. Sci. Lett.*, *242*, 406–414.

Atkinson, J. D., B. J. Murray, M. T. Woodhouse, T. F. Whale, K. J. Baustian, K. S. Carslaw, S. Dobbie, D. O'Sullivan, and T. L. Malkin (2013), The importance of feldspar for ice nucleation by mineral dust in mixed-phase clouds, *Nature*, *498*(7454), 355–358, doi:10.1038/nature12278.

Bacon, M. P. (1984), Glacial to interglacial changes in carbonate and clay sedimentation in the Atlantic Ocean estimated from 230 Th measurements, *Isot. Geosci.*, *2*, 97–111.

Booth, B. B. B., N. J. Dunstone, P. R. Halloran, T. Andrews, and N. Bellouin (2012), Aerosols implicated as a prime driver of twentieth-century North Atlantic climate variability, *Nature*, *484*(7393), 228–U110, doi:10.1038/nature10946.

Bory, A., F. Dulac, C. Moulin, I. Chiapello, P. P. Newton, W. Guelle, C. E. Lambert, and G. Bergametti (2002), Atmospheric and oceanic dust fluxes in the northeastern tropical Atlantic Ocean: How close a coupling?, *Ann. Geophys.*, *20*(12), 2067–2076.

Boucher, O., et al. (2013), Clouds and aerosols, in *Climate Change 2013: The Physical Science Basis. Contribution of Working Group I to the Fifth Assessment Report of the Intergovernmental Panel on Climate Change*, edited by T. F. Stocker et al., Cambridge Univ. Press, Cambridge, U. K., and New York.

Boyd, P. W., et al. (2007), Mesoscale iron enrichment experiments 1993–2005: Synthesis and future directions, *Science*, *315*(5812), 612–617, doi:10.1126/science.1131669.

Bradtmiller, L. I., R. F. Anderson, M. Q. Fleisher, and L. H. Burckle (2007), Opal burial in the equatorial Atlantic Ocean over the last 30 ka: Implications for glacial-interglacial changes in the ocean silicon cycle, *Paleoceanography*, *22*, PA4216, doi:10.1029/2007PA001443.

Castillo, S., T. Moreno, X. Querol, A. Alastuey, E. Cuevas, L. Herrmann, M. Mounkaila, and W. Gibbons (2008), Trace element variation in size-fractionated African desert dusts, *J. Arid Environ.*, *72*(6), 1034–1045, doi:10.1016/j.jaridenv.2007.12.007.

Cheng, H., et al. (2013), Improvements in Th-230 dating, Th-230 and U-234 half-life values, and U-Th isotopic measurements by multi-collector inductively coupled plasma mass spectrometry, *Earth Planet. Sci. Lett.*, *371*, 82–91, doi:10.1016/j.epsl.2013.04.006.

Conway, H., A. Gades, and C. F. Raymond (1996), Albedo of dirty snow during conditions of melt, *Water Resour. Res.*, *32*(6), 1713–1718, doi:10.1029/96WR00712.

Costa, K. M., J. F. McManus, R. F. Anderson, H. Ren, D. M. Sigman, G. Winckler, M. Q. Fleisher, F. Marcantonio, and A. C. Ravelo (2016), No iron fertilization in the equatorial Pacific Ocean during the last ice age, *Nature*, *529*, 519–522, doi:10.1038/nature16453.

Francois, R., M. Frank, M. M. R. van der Loeff, and M. P. Bacon (2004), ^{230}Th normalization: An essential tool for interpreting sedimentary fluxes during the late Quaternary, *Paleoceanography*, *19*, PA1018, doi:10.1029/2003PA000939.

Francois, R., et al. (2007), Comment on "Do geochemical estimates of sediment focusing pass the sediment test in the equatorial Pacific" by Lyle et al, *Paleoceanography*, *22*, PA1216, doi:10.1029/2005PA001235.
Francois, R., and M. P. Bacon (1991), Variations in terrigenous input into the deep equatorial atlantic during the past 24,000 years, *Science*, *251*(5000), 1473–1476, doi:10.1126/science.251.5000.1473.
Gaiero, D. M., F. Brunet, J.-L. Probst, and P. J. Depetris (2007), A uniform isotopic and chemical signature of dust exported from Patagonia: Rock sources and occurrence in southern environments, *Chem. Geol.*, *238*(1–2), 107–120, doi:10.1016/j.chemgeo.2006.11.003.
Ginoux, P., J. M. Prospero, T. E. Gill, N. C. Hsu, and M. Zhao (2012), Global-scale attribution of anthropogenic and natural dust sources and their emission rates based on MODIS DEEP BLUE aerosols products, *Rev. Geophys.*, *50*, RG3005, doi:10.1029/2012RG000388.
Han, Q., J. K. Moore, C. Zender, C. Measures, and D. Hydes (2008), Constraining oceanic dust deposition using surface ocean dissolved Al, *Global Biogeochem. Cycles*, *22*, GB2003, doi:10.1029/2007GB002975.
Hayes, C. T., R. F. Anderson, M. Q. Fleisher, S. Serno, G. Winckler, and R. Gersonde (2013), Quantifying lithogenic inputs to the North Pacific Ocean using the long-lived thorium isotopes, *Earth Planet. Sci. Lett.*, *383*, 16–25, doi:10.1016/j.epsl.2013.09.025
Henderson, G. M., and R. F. Anderson (2003), The U-series toolbox for paleoceanography, *Uranium-Ser. Geochem.*, *52*, 493–531, doi:10.2113/0520493.
Hsieh, Y.-T., G. M. Henderson, and A. L. Thomas (2011), Combining seawater Th-232 and Th-230 concentrations to determine dust fluxes to the surface ocean, *Earth Planet. Sci. Lett.*, *312*(3–4), 280–290, doi:10.1016/j.epsl.2011.10.022.
Hurrell, J. W., et al. (2013), The Community Earth System Model: A framework for collaborative research, *Bull. Am. Meteorol. Soc.*, *94*(9), 1339–1360, doi:10.1175/bams-d-12-00121.1.
Jaccard, S. L., C. T. Hayes, A. Martinez-Garcia, D. A. Hodell, D. A. Anderson, D. M. Sigman, and G. H. Haug (2013), Two modes of change in Southern Ocean productivity over the past million years, *Science*, *339*(6126), 1419–1423, doi:10.1126/science.1227545
Jacobel, A. W., J. F. McManus, R. F. Anderson, and G. Winckler (2016), Large deglacial shifts of the Pacific Intertropical Convergence Zone, *Nat. Commun.*, *7*, 10,449–10,449, doi:10.1038/ncomms10449.
Kanfoush, S. L., D. A. Hodell, C. D. Charles, T. P. Guilderson, P. G. Mortyn, and U. S. Ninnemann (2000), Millennial-scale instability of the antarctic ice sheet during the last glaciation, *Science*, *288*(5472), 1815–1818, doi:10.1126/science.288.5472.1815.
Kelemen, P. B., K. Hanghoj, and A. R. Greene (2004), One view of the geochemistry of subduction-related magmatic arcs, with an emphasis on primitive andesite and lower crust, in *Treatise on Geochemistry*, vol. 3, edited by H. D. Holland and K. K. Turekian, pp. 593–659, Elsevier, Amsterdam.
Kienast, S. S., M. Kienast, A. C. Mix, S. E. Calvert, and R. François (2007), Thorium-230 normalized particle flux and sediment focusing in the Panama Basin region during the last 30,000 years, *Paleoceanography*, *22*, PA2213, doi:10.1029/2006PA001357.
Kienast, S. S., T. Friedrich, N. Dubois, P. S. Hill, A. Timmermann, A. C. Mix, and M. Kienast (2013), Near collapse of the meridional SST gradient in the eastern equatorial Pacific during Heinrich Stadial 1, *Paleoceanography*, *28*, 663–674, doi:10.1002/2013PA002499.
Klein, E. M. (2004), *Geochemistry of the Igneous Oceanic Crust in Treatise on Geochemistry*, vol. 3, edited by H. D. Holland and K. K. Turekian, pp. 443–463, Elsevier, Amsterdam.
Kohfeld, K. E. (2002), DIRTMAP Version 2. LGM and Late Holocene Eolian Fluxes from Ice Cores Marine Sediment Traps, Marine Sediments, and Loess DepositsGBP PAGES/World Data Center for Paleoclimatology NOAA/NGDC Paleoclimatology Program, Boulder Colo., Data Contribution Series #2002-045.
Kohfeld, K. E., and S. P. Harrison (2001), DIRTMAP: The geological record of dust, *Earth Sci. Rev.*, *54*, 81–114.
Kohfeld, K. E., R. M. Graham, A. M. de Boer, L. C. Sime, E. W. Wolff, C. Le Quere, and L. Bopp (2013), Southern Hemisphere westerly wind changes during the Last Glacial Maximum: Paleo-data synthesis, *Quat. Sci. Rev.*, *68*, 76–95, doi:10.1016/j.quascirev.2013.01.017.
Kok, J. F. (2011), A scaling theory for the size distribution of emitted dust aerosols suggests climate models underestimate the size of the global dust cycle, *Proc. Natl. Acad. Sci. U.S.A.*, *108*(3), 1016–1021, doi:10.1073/pnas.1014798108.
Lamy, F., R. Gersonde, G. Winckler, O. Esper, A. Jaeschke, G. Kuhn, J. Ullermann, A. Martinez-Garcia, F. Lambert, and R. Kilian (2014), Increased dust deposition in the Pacific Southern Ocean during glacial periods, *Science*, *343*(6169), 403–407, doi:10.1126/science.1245424.
Lawrence, C. R., and J. C. Neff (2009), The contemporary physical and chemical flux of aeolian dust: A synthesis of direct measurements of dust deposition, *Chem. Geol.*, *267*(1–2), 46–63, doi:10.1016/j.chemgeo.2009.02.005.
Lebti, P. P., J. C. Thouret, G. Worner, and M. Fornari (2006), Neogene and Quaternary ignimbrites in the area of Arequipa, Southern Peru: Stratigraphical and petrological correlations, *J. Volcanol. Geotherm. Res.*, *154*(3–4), 251–275, doi:10.1016/j.jvolgeores.2006.02.014.
Lopez, G. I., F. Marcantonio, M. Lyle, and J. Lynch-Stieglitz (2015), Dissolved and particulate Th-230-Th-232 in the Central Equatorial Pacific Ocean: Evidence for far-field transport of the East Pacific Rise hydrothermal plume, *Earth Planet. Sci. Lett.*, *431*, 87–95, doi:10.1016/j.epsl.2015.09.019.
Maher, B. A., J. M. Prospero, D. Mackie, D. Gaiero, P. P. Hesse, and Y. Balkanski (2010), Global connections between aeolian dust, climate and ocean biogeochemistry at the present day and at the Last Glacial Maximum, *Earth Sci. Rev.*, *99*(1–2), 61–97, doi:10.1016/j.earscirev.2009.12.001.
Mahowald, N. M., A. R. Baker, G. Bergametti, N. Brooks, R. A. Duce, T. D. Jickells, N.¨n. Kubilay, J. M. Prospero, and I. Tegen (2005), Atmospheric global dust cycle and iron inputs to the ocean, *Global Biogeochem. Cycles*, *19*, GB4025, doi:10.1029/2004GB002402.
Mahowald, N. M., D. R. Muhs, S. Levis, P. J. Rasch, M. Yoshioka, C. S. Zender, and C. Luo (2006), Change in atmospheric mineral aerosols in response to climate: Last glacial period, preindustrial, modern, and doubled carbon dioxide climates, *J. Geophys. Res.*, *111*, D10202, doi:10.1029/2005JD006653.
Mahowald, N. M., et al. (2010), Observed 20th century desert dust variability: Impact on climate and biogeochemistry, *Atmos. Chem. Phys.*, *10*(22), 10,875–10,893, doi:10.5194/acp-10-10875-2010.
Mahowald, N., S. Albani, J. F. Kok, S. Engelstaeder, R. Scanza, D. S. Ward, and M. G. Flanner (2014), The size distribution of desert dust aerosols and its impact on the Earth system, *Aeolian Res.*, *15*, 53–71, doi:10.1016/j.aeolia.2013.09.002.
Marcantonio, F., M. Lyle, and R. Ibrahim (2014), Particle sorting during sediment redistribution processes and the effect on 230Th-normalized mass accumulation rates, *Geophys. Res. Lett.*, *41*, 5547–5554, doi:10.1002/2014GL060477.
Maring, H., Savoie, D. L., Izaguirre, M. A., Custals, L., and Reid, J. S. (2003), Mineral dust aerosol size distribution change during atmospheric transport, *J. Geophys. Res.*, *108*(D19), 8592, doi:10.1029/2002JD002536.
Martin, J. M., and M. Meybeck (1979), Elemental mass-balance of material carried by major world rivers, *Mar. Chem.*, *7*(3), 173–206, doi:10.1016/0304-4203(79)90039-2.
Martinez-Garcia, A., A. Rosell-Mele, W. Geibert, R. Gersonde, P. Masque, V. Gaspari, and C. Barbante (2009), Links between iron supply, marine productivity, sea surface temperature, and CO_2 over the last 1.1 Ma, *Paleoceanography*, *24*, PA1207, doi:10.1029/2008PA001657.
Martinez-Garcia, A., A. Rosell-Mele, S. L. Jaccard, W. Geibert, D. M. Sigman, and G. H. Haug (2011), Southern Ocean dust-climate coupling over the past four million years, *Nature*, *476*(7360), 312–U141, doi:10.1038/nature10310.

McCave, I. N. (1986), Local and global aspects of the bottom nepheloid layers in the world ocean, *Neth. J. Sea Res.*, *20*, 167–181.
McGee, D., F. Marcantonio, and J. Lynch-Stieglitz (2007), Deglacial changes in dust flux in the eastern equatorial Pacific, *Earth Planet. Sci. Lett.*, *257*, 215–230.
McGee, D., F. Marcantonio, J. F. McManus, and G. Winckler (2010), The response of excess ^{230}Th and extraterrestrial ^{3}He to sediment redistribution at the Blake Ridge, western North Atlantic, *Earth Planet. Sci. Lett.*, *299*, 138–149.
McGee, D., P. B. deMenocal, G. Winckler, J. B. W. Stuut, and L. I. Bradtmiller (2013), The magnitude, timing and abruptness of changes in North African dust deposition over the last 20,000 yr, *Earth Planet. Sci. Lett.*, *371*, 163–176, doi:10.1016/j.epsl.2013.03.054.
McGee, D., et al. (2016), Tracking eolian dust with helium and thorium: Impacts of grain size and provenance, *Geochim. Cosmochim. Acta*, *175*, 47–67.
Moreno, T., X. Querol, S. Castillo, A. Alastuey, E. Cuevas, L. Herrmann, M. Mounkaila, J. Elvir, and W. Gibbons (2006), Geochemical variations in aeolian mineral particles from the Sahara-Sahel Dust Corridor, *Chemosphere*, *65*(2), 261–270, doi:10.1016/j.chemosphere.2006.02.052.
Muhs, D. R., J. R. Budahn, J. M. Prospero, and S. N. Carey (2007), Geochemical evidence for African dust inputs to soils of western Atlantic islands: Barbados, the Bahamas, and Florida, *J. Geophys. Res.*, *112*, F02009, doi:10.1029/2005JF000445.
Mulitza, S., et al. (2010), Increase in African dust flux at the onset of commercial agriculture in the Sahel region, *Nature*, *466*(7303), 226–228, doi:10.1038/nature09213.
Murray, R. W., M. Leinen, D. W. Murray, A. C. Mix, and C. W. Knowlton (1995), Terrigenous Fe input and biogenic sedimentation in the glacial and interglacial equatorial Pacific Ocean, *Global Biogeochem. Cycles*, *9*(4), 667–684, doi:10.1029/95GB02833.
Olivarez, A. M., R. M. Owen, and D. K. Rea (1991), Geochemistry of eolian dust in pacific pelagic sediments—Implications for paleoclimatic interpretations, *Geochim. Cosmochim. Acta*, *55*(8), 2147–2158, doi:10.1016/0016-7037(91)90093-k.
Orsi, A. H., T. Whitworth, and W. D. Nowlin (1995), On the meridional extent and fronts of the antarctic circumpolar current, *Deep-Sea Res. Part I-Oceanogr. Res. Pap.*, *42*(5), 641–673, doi:10.1016/0967-0637(95)00021.
Pourmand, A., F. Marcantonio, and H. Schulz (2004), Variations in productivity and eolian fluxes in the northeastern Arabian Sea during the past 110 ka, *Earth Planet. Sci. Lett.*, *221*(1–4), 39–54, doi:10.1016/s0012-821x(04)00109-8.
Prospero, J. M., and E. Bonatti (1969), Continental dust in the atmosphere of the eastern equatorial Pacific, *J. Geophys. Res.*, *74*(13), 3362–3371, doi:10.1029/JC074i013p03362.
Prospero, J. M., R. T. Nees, and M. Uematsu (1987), Deposition rate of particulate and dissolved aluminum derived from Saharan dust in precipitation at Miami, Florida, *J. Geophys. Res.*, *92*(D12), 14,723–14,731, doi:10.1029/JD092iD12p14723.
Pye, K. (1995), The nature, origin and accumulation of loess, *Quat. Sci. Rev.*, *14*(7–8), 653–667, doi:10.1016/0277-3791(95)00047-x.
Rea, D. K. (1994), The paleoclimatic record provided by eolian deposition in the deep sea: The geologic history of wind, *Rev. Geophys.*, *32*(2), 159–195, doi:10.1029/93RG03257.
Rudnick, R. L., and S. Gao (2004), Composition of the continental crust, in *Treatise on Geochemistry*, vol. 3, edited by H. D. Holland and K. K. Turekian, pp. 1–64, Elsevier, Amsterdam.
Rühlemann, C., and M. Butzin (2006), Alkenone temperature anomalies in the Brazil-Malvinas Confluence area caused by lateral advection of suspended particulate material, *Geochem. Geophys. Geosyst.*, *7*, Q10015, doi:10.1029/2006GC001251.
Schulz, M., et al. (2012), Atmospheric transport and deposition of mineral dust to the ocean: Implications for research needs, *Environ. Sci. Technol.*, *46*(19), 10,390–10,404, doi:10.1021/es300073u.
Serno, S., G. Winckler, R. F. Anderson, C. T. Hayes, D. McGee, B. Machalett, H. Ren, S. M. Straub, R. Gersonde, and G. H. Haug (2014), Eolian dust input to the subarctic North Pacific, *Earth Planet. Sci. Lett.*, *387*, 252–263, doi:10.1016/j.epsl.2013.11.008.
Siegel, D. A., and W. G. Deuser (1997), Trajectories of sinking particles in the Sargasso Sea: Modeling of statistical funnels above deep-ocean sediment traps, *Deep-Sea Res. Part I-Oceanogr. Res. Pap.*, *44*(9–10), 1519–1541, doi:10.1016/s0967-0637(97)00028-9.
Singh, A. K., F. Marcantonio, and M. Lyle (2011), Sediment focusing in the Panama Basin, eastern equatorial Pacific, *Earth Planet. Sci. Lett.*, *309*, 33–44.
Stuart, K. M., and D. G. Long (2011), Tracking large tabular icebergs using the SeaWinds Ku-band microwave scatterometer, *Deep-Sea Res. Part II-Topical Stud. Oceanogr.*, *58*(11–12), 1285–1300, doi:10.1016/j.dsr2.2010.11.004.
Taylor, S. R., and S. M. McClennan (1985), *The continental crust: Its composition and evolution*, Blackwell Scientific Publ., Oxford.
van Sebille, E., P. Scussolini, J. V. Durgadoo, F. J. C. Peeters, A. Biastoch, W. Weijer, C. Turney, C. B. Paris, and R. Zahn (2015), Ocean currents generate large footprints in marine palaeoclimate proxies, *Nat. Commun.*, *6*, doi:10.1038/ncomms7521.
Ward, D. S., N. M. Mahowald, and S. Kloster (2014), Potential climate forcing of land use and land cover change, *Atmos. Chem. Phys.*, *14*(23), 12,701–12,724, doi:10.5194/acp-14-12701-2014.
Werner, M., I. Tegen, S. P. Harrison, K. E. Kohfeld, I. C. Prentice, Y. Balkanski, H. Rodhe, and C. Roelandt (2002), Seasonal and interannual variability of the mineral dust cycle under present and glacial climate conditions, *J. Geophys. Res.*, *107*(D24), 4744, doi:10.1029/2002JD002365.
Winckler, G., R. F. Anderson, and P. Schlosser (2005), Equatorial Pacific productivity and dust flux during the mid-Pleistocene climate transition, *Paleoceanography*, *20*, PA4025, doi:10.1029/2005PA001177.
Winckler, G., R. F. Anderson, M. Q. Fleischer, D. McGee, and N. Mahowald (2008), Covariant glacial-interglacial dust fluxes in the equatorial Pacific and Antarctica, *Science*, *320*, 93–96.
Winckler, G., R. F. Anderson, S. L. Jaccard, and F. Marcantonio (2016), Ocean dynamics, not dust, have controlled equatorial Pacific productivity over the past 500,000 years, *Proc. Natl. Acad. Sci. U.S.A.*, *113*(22), 6119–6124, doi:10.1073/pnas.1600616113.
Woodard, S. C., D. J. Thomas, and F. Marcantonio (2012), Thorium-derived dust fluxes to the tropical Pacific Ocean, 58 Ma, *Geochim. Cosmochim. Acta*, *87*, 194–209, doi:10.1016/j.gca.2012.03.035.
Zender, C., Bian, H., and Newman, D. (2003), Mineral Dust Entrainment and Deposition (DEAD) model: Description and 1990s dust climatology, *J. Geopys. Res.*, *108*(D14), 4461, doi:10.1029/2002JD002775.